



HAL
open science

Copper nanoparticles supported on ZIF-8: comparison of Cu(II) reduction processes and application as benzyl alcohol oxidation catalysts

Yifan Zan, Ferdaous Ben Romdhane, Antoine Miche, Christophe Méthivier, Jean-Marc Krafft, Claude Jolival, Julien Reboul

► To cite this version:

Yifan Zan, Ferdaous Ben Romdhane, Antoine Miche, Christophe Méthivier, Jean-Marc Krafft, et al.. Copper nanoparticles supported on ZIF-8: comparison of Cu(II) reduction processes and application as benzyl alcohol oxidation catalysts. *ACS Applied Materials & Interfaces*, 2023, 15 (32), pp.38716-38728. 10.1021/acsami.3c08906 . hal-04192093

HAL Id: hal-04192093

<https://hal.science/hal-04192093v1>

Submitted on 31 Aug 2023

HAL is a multi-disciplinary open access archive for the deposit and dissemination of scientific research documents, whether they are published or not. The documents may come from teaching and research institutions in France or abroad, or from public or private research centers.

L'archive ouverte pluridisciplinaire **HAL**, est destinée au dépôt et à la diffusion de documents scientifiques de niveau recherche, publiés ou non, émanant des établissements d'enseignement et de recherche français ou étrangers, des laboratoires publics ou privés.

Copper nanoparticles supported on ZIF-8: comparison of Cu(II) reduction processes and application as benzyl alcohol oxidation catalysts

Yifan Zan¹, Ferdaous Ben Romdhane², Antoine Miche¹, Christophe Méthivier¹, Jean-Marc Krafft¹, Claude Jolival^{1}, Julien Reboul^{1*}*

¹ Sorbonne Université, CNRS, Laboratoire de Réactivité de Surface (LRS), 4 Place Jussieu, 75005 Paris, France

² Fédération de Chimie et Matériaux de Paris- Centre (FCMat), 4 Place Jussieu, 75005 Paris, France

KEYWORDS. Copper nanoparticles, ZIF-8, Cu(II) reduction process, nanoparticle location, aerobic alcohol oxidation, ZnO impurities

ABSTRACT. We report the synthesis of a stable heterogeneous catalyst based on copper metal nanoparticles with oxidized surface supported on ZIF-8 for the oxidation of benzyl alcohol under mild temperature and using air as sustainable oxygen source as well as for the implementation of tandem “one-pot” catalytic system allowing the sustainable synthesis of benzylidene

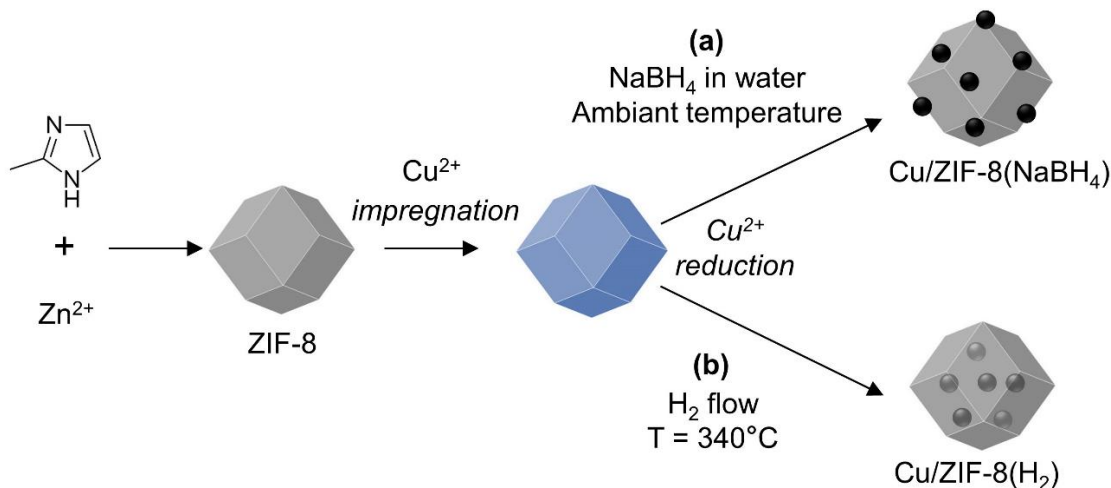
malononitrile. The influence of the reduction process applied to form the nanoparticle upon the catalyst texture and its performances was extensively examined. After ZIF-8 impregnation with a copper chloride precursor, the reduction of cupric ions into Cu^0 nanoparticles was carried out according to two procedures: (i) by soaking the solid into a solution of NaBH_4 and (ii) by submitting it to a flow of gaseous H_2 at 340°C . The in-depth physicochemical characterization and comparison of the resulting two types of Cu/ZIF-8 materials reveal significant differences: the reduction with NaBH_4 led to the formation of 16 nm sized Cu^0 nanoparticles (NP) mainly localized on the external surface of the ZIF-8 crystals together with ZnO nanocrystallites, while the reduction under H_2 flow results in Cu^0 nanoparticles with a mean size of 22 nm embedded within the bulk of ZIF-8 crystals. More, when NaBH_4 was used to reduce cupric ions, ZnO particles were highlighted by high-resolution microscopy imaging. Formation of ZnO impurities was confirmed by the photoluminescence analysis of ZIF-8 after NaBH_4 treatment. In contrast, ZnO was not detected on ZIF-8 treated with H_2 . Both types of the Cu^0 NPs supported on ZIF-8 were found to be active as catalysts towards the aerobic oxidation of benzyl alcohol under moderate temperature ($T < 80^\circ\text{C}$) and using air as sustainable O_2 source. Benzaldehyde yields of 66% and selectivity superior to 90% were obtained with Cu/ZIF-8 catalyst prepared under H_2 flow after 24h under these conditions. The same material could be recycled 5 times without loss of activity, unlike the catalysts synthesized with NaBH_4 , as a result of the leaching of the surface copper NPs over the consecutive catalytic cycles. Finally, the most stable catalyst was successfully implemented in a tandem “one-pot” catalytic system associating benzyl alcohol oxidation and Knoevenagel condensation to synthesize benzylidene malononitrile.

1. Introduction

Copper-based catalysts are of high potential interest among transition metal for the development of economic and sustainable oxidation catalytic systems. They afford promising alternatives to the classic oxidation methods using stoichiometric quantities of toxic inorganic oxidants, such as manganese dioxide, chromium (VI), the Swern or Dess-Martin reagents¹ and to more virtuous but still highly expensive catalytic systems based on the use of precious metals, such as gold and platinum.^{2,3} A variety of copper (II) complexes were recently reported allowing the oxidation of alcohols under mild conditions using O₂ or hydroperoxide as sustainable alternative oxidants.⁴ Among these catalytic systems, copper complexes associated with a nitroxyl co-catalyst, typically the commercially available and stable 2,2,6,6-tetramethylpiperidine-1-oxyl radical (TEMPO), were shown to be particularly efficient for the selective aerobic oxidation of benzylic, allylic, and aliphatic alcohols under mild temperatures and using pure O₂ or even ambient air.⁵ However, these copper complexes imply the use of relatively expensive specific organic ligands, whose synthesis can be tedious.⁶ Furthermore, the homogeneous character of these copper catalytic systems inherently entails problems related to their separation and recycling, as well their stability. These issues were recently addressed by combining TEMPO with copper oxide or surface-oxidized copper metal nanoparticles supported on various supports, resulting in robust and active heterogeneous catalytic systems.^{7,8,9,10} Metal-Organic Frameworks (MOFs) were shown to be excellent support for metallic and metal oxide nanoparticles mainly because their extremely high surface area promotes the efficient dispersion of metal precursors within the crystal bulk, resulting in highly dispersed nanoparticles after a metal cation reduction step. Among them, ZIF-8, a prototypical MOF composed of a zinc-imidazolate framework was particularly studied as support for a variety of metals nanoparticles (Au, Pd, Ru, Cu...) ¹¹ due to its high surface area, its three-

dimensional structure made of interconnected nanocages and relative stability in a wide range of reaction conditions, including basic aqueous media. Herein we report the immobilization of copper metal nanoparticles (NPs) on ZIF-8 and their use as stabilized copper-based heterogeneous catalyst systems capable to selectively oxidize benzylic alcohols in the presence of TEMPO and an organic base (4-dimethylaminopyridine, DMAP) under mild temperature and with air as oxidant source. A particular attention was given to the method used to reduce the copper cations dispersed within the pores of ZIF-8. Two traditional reduction methods were compared: (i) a wet route using an aqueous NaBH₄ solution and (ii) a dry route achieved under H₂ flow at the reduction temperature of the metal precursors (determined by H₂-TPR) (Scheme 1). The resulting two types of catalyst were carefully characterized and their performances in the oxidation of benzyl alcohol were compared. Finally, a tandem catalytic system, combining alcohol oxidation and Knoevenagel catalysis in a one-pot synthesis process, was implemented with the most promising Cu/ZIF catalyst relative to the oxidation step, taking advantage of Cu NP activity and of the basic properties of both ZIF-8 imidazolate linkers and DMAP required in the Knoevenagel coupling step.

Scheme 1. Schematic representation of the formation of Cu/ZIF-8 nanocomposites following the two Cu^{2+} reduction methods compared in this work: (a) using NaBH_4 and (b) using H_2 .



2. Experimental section

2.1 Chemicals.

Chemicals were from commercial source and used without any further purification. Copper (II) chloride dihydrate ($\text{CuCl}_2 \cdot 2\text{H}_2\text{O}$, $\geq 99\%$), zinc nitrate hexahydrate ($\text{Zn}(\text{NO}_3)_2 \cdot 6\text{H}_2\text{O}$, $\geq 99\%$), 2-methylimidazole (2-mim, 99%), sodium borohydride (NaBH_4 , 98%), 2,2,6,6-tetramethylpiperidiny-1-oxy (TEMPO, 98%), 4-dimethylaminopyridine (DMAP, $\geq 99\%$), benzyl alcohol ($\geq 99\%$) and caffeine were purchased from Sigma-Aldrich. Benzaldehyde (99+%), acetonitrile (99.8+%) was purchased from Alfa Aesar. Methanol (analytical grade) and ethanol (99.98%) were purchased from VWR.

2.2 Synthesis of ZIF-8.

ZIF-8 was synthesized following a procedure described by Astruc et al. in the literature with minor modifications.¹² In brief, 13.3 mmol of $\text{Zn}(\text{NO}_3)_2 \cdot 6\text{H}_2\text{O}$ was dissolved in 100 mL of

methanol. Then, 50 mmol of 2-methylimidazole dissolved in 100 mL methanol was added slowly. The mixture was maintained at 30 °C and aged for 24 hours. The product was collected by centrifugation and washed 3 times with 30 mL of methanol. The obtained material was heated at 100 °C under vacuum overnight and the obtained ZIF-8 solid stored at room temperature before further use.

2.3 Synthesis of Cu/ZIF-8.

The Cu²⁺/ZIF-8 was prepared by soaking 114 mg of ZIF-8 in 10 ml of a 0.25 mmol CuCl₂·2H₂O solution in methanol. The suspension was stirred for 24 hours. The purple solid (Cu²⁺/ZIF-8) was then harvested by filtration and washed with 30 mL of methanol.

Cu²⁺/ZIF-8 was then reduced either with NaBH₄ or H₂ to produce metal copper NPs. Reduction with NaBH₄ was achieved by re-dispersing Cu²⁺/ZIF-8 into 10 mL of water and adding 5 mL of fresh aqueous solution of NaBH₄ (240 mM, 4 equivalents) drop-wise under vigorous stirring. The stirring lasted for 4 hours. A deep blue powder was collected by filtration. Reduction with H₂ was achieved by treating Cu²⁺/ZIF-8 with 100 mL/min H₂ flow at 340 °C for 20 minutes.

Regardless of the reduction method, the collected Cu/ZIF-8 particles were washed with 10 mL of methanol for 3 times. Then, they were dried at 90 °C under vacuum overnight before its characterization and catalytic assessment. Solids reduced by using NaBH₄ are denoted as Cu/ZIF-8(NaBH₄) and those reduced under H₂ gaseous flow as Cu/ZIF-8(H₂).

2.4 Characterization.

Powder X-ray diffraction (PXRD) of ZIF-8, Cu²⁺/ZIF-8, Cu/ZIF-8(NaBH₄) and Cu/ZIF-8(H₂) were performed using a Bruker D8 Advance diffractometer (Cu K α =1.5406 Å). The N₂

physisorption analyses were performed using a Belsorp MAX instrument. The samples were pretreated by vacuum at 100 °C for 18 hours, and the textural parameters were calculated according to the Brunauer, Emmett and Teller (BET) method.

Imaging of the samples was performed by conventional transmission electron microscopy (TEM) using a JEOL 1011 operating at 100 kV. High-resolution transmission electron microscopy (HRTEM) was carried out using a JEOL 2100Plus UHR microscope operating at 200 kV. Samples were dispersed in ethanol, and the resulting solution dropped onto a carbon film supported on a nickel grid. Scanning transmission electron microscopy (STEM) images using a high-angle annular dark-field (HAADF) detector were also recorded. Analytic investigations were performed with an energy dispersive X-ray (EDX) spectrometer attached to the microscope column.

XPS analyses were performed using an Omicron Argus X-ray photoelectron spectrometer, equipped with a monochromated AlK α radiation source ($h\nu = 1486.6$ eV) and a 280 W electron beam power. The emission of photoelectrons from the sample was analyzed at a takeoff angle of 45° under ultra-high vacuum conditions ($\leq 10^{-9}$ mbar). Spectra were recorded with a 100 eV pass energy for the survey scan and 20 eV pass energy for the C 1s, O 1s, N 1s, Cu 2p and Zn 2p regions and element peak intensities were corrected by Scofield factors. The peak areas of Cu 2p were determined after subtraction of a U 2 TOUGAARD background. The spectra were fitted using Casa XPS v.2.3.15 software (Casa Software Ltd, U.K.) and applying a Gaussian/Lorentzian ratio G/L equal to 70/30.

Zn and Cu contents of the synthesized catalysts were determined by inductively coupled plasma atomic emission spectroscopy (ICP-OES) using an Agilent ICP-OES 5100 SVDV equipment. The hydrogen temperature-programmed reduction (H₂-TPR) of ZIF-8 and Cu²⁺/ZIF-8 was performed using a Micromeritics AutoChem 2910.

Photoluminescence measurements were performed with a Horiba Jobin Yvon Fluorolog 3 spectrofluorimeter equipped with a 450 W Xe lamp as an excitation source. Solids ZIF-8, ZIF-8 treated with NaBH_4 (ZIF-8(NaBH_4)) and ZIF-8 treated with H_2 (ZIF-8(H_2)) were placed in a suprasil quartz cell with 5 mm external diameter and 4mm internal diameter. Excitation was set at $\lambda_{\text{exc}} = 335$ nm and emission spectrum was recorded between 350 and 650 nm.

2.5 Catalytic aerobic oxidation of alcohols.

The catalytic aerobic oxidation of alcohols to the corresponding aldehydes was performed in a 5 mL round-bottom flask sealed with a septum equipped with a balloon. In a typical reaction, 0.2 mmol (1 wt. %) of alcohol, 0.01 mmol (5 mol % to the substrate) of TEMPO and 0.1 mmol of DMAP were dissolved in 2 mL of acetonitrile. Then, 5 mg of catalyst (based on copper, 10 mol % to the substrate) was added. The suspension was treated under ultrasound for 2 minutes to disperse the catalyst within the reaction solution. The reaction was performed under stirring at 600 rpm at constant temperatures maintained by oil bath. The atmosphere was set to oxygen or air by filling the balloon connected to the reaction vessel with the corresponding gas. In the case of O_2 , the flask was blown by O_2 before adding the catalyst. After the catalytic test, the catalyst was recovered by centrifugation and washed with 2 mL of methanol for 3 times. Recyclability test was achieved after reactivating the catalyst at 90 °C under vacuum. The reaction solution was analyzed by high performance liquid chromatography (HPLC, 1260 Infinity II by Agilent) equipped with a Beckman Coulter ultrasphere ODS column (150 x 4.6 mm, 5 μm) and a diode-array detector (DAD). The mobile phase was the mixture of acetonitrile and water (v:v=50:50). The concentration of reactants and products were determined using calibration curves and caffeine as an internal standard to correct deviations due to solvent volume changes because of its partial evaporation.

One-pot sequential oxidation/Knoevenagel condensation reaction was achieved by mixing in a 10 mL round-bottom flask 0.2 mmol (1 wt. %) of benzyl alcohol, 0.01 mmol (5 mol % to the substrate) of TEMPO, 0.1 mmol of DMAP and 2 mL of acetonitrile. Then, 5 mg of catalyst (based on copper, 10 mol% to the substrate) was added and dispersed by ultrasonication (1 min). A balloon filled with air was connected to the round flask and the reaction was allowed to proceed under magnetic stirring at $T = 70^{\circ}\text{C}$ until the alcohol conversion reached an almost constant value. An amount of 0.33 mmol of malononitrile was then added to the reaction mixture that was placed under stirring at $T = 70^{\circ}\text{C}$. The same protocol was also achieved without the addition of DMAP.

3. Results and discussion

3.1 Synthesis and characterization of the catalysts

The copper nanoparticles supported on ZIF-8 crystals were prepared according to the procedure illustrated in Scheme 1. The diffraction pattern of the purple powder recovered after ZIF-8 impregnation with the copper chloride solution agrees with that of the pristine ZIF-8 (Figure 1). It shows that impregnation does not affect the crystal structure of ZIF-8. On the other hand, a drastic reduction of BET specific surface from $1621\text{ cm}^2\cdot\text{g}^{-1}$ to $745\text{ cm}^2\cdot\text{g}^{-1}$ and of pore volume (from $0.64\text{ cm}^3\cdot\text{g}^{-1}$ to $0.43\text{ cm}^3\cdot\text{g}^{-1}$) were evidenced by N_2 sorption analysis at 77K after CuCl_2 impregnation, suggesting the partial filling of ZIF-8 pores by the Cu^{2+} precursor (Figure 2 and Table 1).

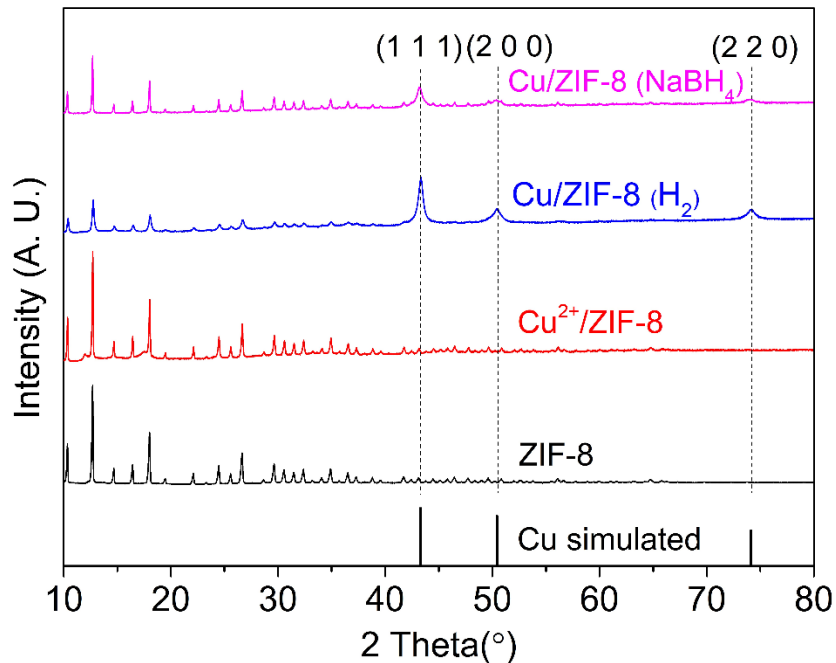


Figure 1. XRD patterns of ZIF-8, $\text{Cu}^{2+}/\text{ZIF-8}$, $\text{Cu}/\text{ZIF-8}(\text{NaBH}_4)$ and $\text{Cu}/\text{ZIF-8}(\text{H}_2)$. The simulated XRD pattern of Cu^0 is also shown for comparison.

Reducibility of copper species adsorbed within ZIF-8 pores was then studied by TPR analysis (Figure S1). The TPR profile of the impregnated material shows only one well-defined peak centered at $T = 340^\circ\text{C}$, incidentally proving the existence of only one type of Cu^{2+} species strongly interacting with the framework of ZIF-8. The purple color of the material after impregnation supports the hypothesis of Cu^{2+} cations strongly interacting with the imidazolate linkers of the hybrid network, namely by the formation of coordination bonds, as copper-imidazolate complexes with a purple color were reported in the literature.¹³ The impregnated $\text{Cu}^{2+}/\text{ZIF-8}$ was then further reduced by two methods (Scheme 1): either (a) under a stream of H_2 at $T = 340^\circ\text{C}$ (the reduction temperature determined by TPR analysis) or (b) by immersing the impregnated ZIF-8 in an aqueous solution of NaBH_4 under stirring. The obtained solids are denoted as $\text{Cu}/\text{ZIF-8}(\text{H}_2)$ or

Cu/ZIF-8(NaBH₄), respectively in the following. Copper contents of Cu/ZIF-8(NaBH₄) and Cu/ZIF-8(H₂) were 21.7 wt. % and 22.4 wt. % as measured by ICP-OES analysis.

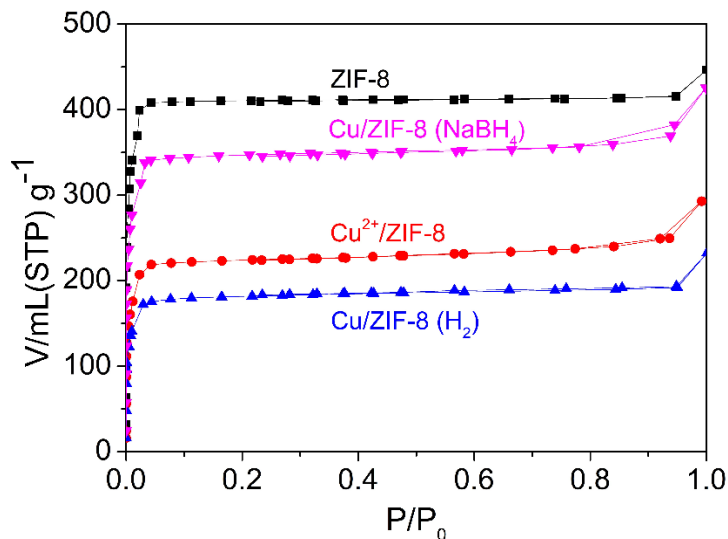


Figure 2. N₂ adsorption isotherms of ZIF-8, Cu²⁺/ZIF-8, Cu/ZIF-8(NaBH₄) and Cu/ZIF-8(H₂).

Table 1. Textural properties of ZIF-8, Cu²⁺/ZIF-8, Cu/ZIF-8(NaBH₄) and Cu/ZIF-8(H₂).

Samples	A _{BET} (cm ² .g ⁻¹) ^a	V _P (cm ³ .g ⁻¹) ^b	d _{Cu} (nm) ^c
ZIF-8	1621	0.64	-
Cu ²⁺ /ZIF-8	745	0.43	-
Cu/ZIF-8(NaBH ₄)	1302	0.62	16 (18)
Cu/ZIF-8(H ₂)	638	0.33	22 (18)

^a BET surface area

^b Pore volume

^c Average Cu crystallite size determined using TEM analysis (the average size determined by Scherrer equation using the (111) peak is indicated into bracket)

After reduction, the PXRD patterns of both Cu/ZIF-8(H₂) and Cu/ZIF-8(NaBH₄) clearly show three additional peaks at 43.4°, 55.5° and 74°, which can be assigned to the (111), (200) and (220) planes of Cu⁰, respectively, indicating the successful formation of Cu⁰ nanoparticles with both reduction methods (Figure 2). It is also noteworthy that a significant decrease of the ZIF-8 diffraction peaks intensity was observed, suggesting losses of crystallinity of the MOF. The discrepancy is even more pronounced in the case of the use of H₂ as a reducing agent. For the latter materials, reduction under H₂ flow results in a reduction of the BET surface area and pore volume to 638 m².g⁻¹ and 0.33 cm³.g⁻¹, respectively (Figure 2, Table 1). In contrast, the opposite trend is observed when NaBH₄ is used as reductant. In this case, surface area and pore volume of the reduced material increase to 1302 m².g⁻¹ and 0.62 cm³.g⁻¹, respectively (Figure 2 and Table 1), ie textural parameters very close to those determined for ZIF-8 alone. Such a result would be in line with the assumption that in case of Cu/ZIF-8(H₂) materials, the Cu⁰ NPs are located inside the ZIF-8 porosity whereas for Cu/ZIF-8(NaBH₄), NPs could be on the external surface of ZIF-8.

TEM imaging was then performed to investigate the morphology, size, dispersion and localization of copper nanoparticles in the two Cu/ZIF-8(NaBH₄) and Cu/ZIF-8(H₂) samples (Figures 3 and 4). A representative image of Cu/ZIF-8(NaBH₄) is shown in Figure 3a, highlighting the presence of particles dispersed on the external surface of the ZIF-8 crystals whose size is mainly in the range between 5 to 80 nm with a mean size of 16 nm (histogram shown in Figure S2a). HRTEM images of most of these nanoparticles (Figure 3a right) display lattice fringes with interplanar spacings of 0.21 nm corresponding to the (100) planes of metal copper (JCPDS 04-0836). The formation of the Cu⁰ nanoparticles dispersed on the external surface of ZIF-8 is confirmed by HAADF, the Cu nanoparticles clearly appearing as bright dots, and STEM-EDX mapping (Figure 3b). Noteworthy, HRTEM imaging also highlights some nanocrystals with ill-

defined shape in addition to the Cu⁰ nanoparticles. These latter particles are characterized by lattice fringes with interplanar spacings of 0.28 nm corresponding to the (100) atomic plane of wurtzite ZnO (JCPDS 36-1451) (additional HRTEM images of Cu/ZIF-8(NaBH₄) are available in Figure S3 and a STEM image showing ZnO nanocrystallites on ZIF-8 is given in Figure S4).

In order to clarify the role of NaBH₄ upon the formation of ZnO only during the reduction process, imaging of ZIF-8 crystals alone (ie without any cupric ions) after soaking in pure water or in a NaBH₄ aqueous solution was compared (Figure S5). No ZnO particles were detected on ZIF-8 soaked in pure water while ZnO crystallites were observed on the ZIF-8 treated with NaBH₄. In such conditions, ZIF-8 partly dissolve, leading to the formation of ZnO particles as a result of the presence of strongly basic and nucleophilic metaborate anions (BO₂⁻) produced during the hydrolysis of NaBH₄ (according to the reaction: $\text{BH}_4^- + 2\text{H}_2\text{O} \rightarrow \text{BO}_2^- + 4\text{H}_2$).¹⁴ An increase of the pH from 8.3 to 10 was indeed measured during the NaBH₄ reduction process of cupric ions. However, no discrepancy of ZIF-8 crystallinity was observed by PXRD of the MOF. Furthermore, no ZnO could be detected by this characterization method (Figure S6). It can be hypothesized that either the ZnO content of the sample is too low, or crystallites are too small to be detected by XRD analysis. This may explain why the formation of such surface ZnO nanoparticles was never reported so far in studies dealing with the synthesis of metal nanoparticles supported on ZIF-related materials using NaBH₄ as reducing agent.^{15,16,17,18,19,20} Formation of ZnO impurities under NaBH₄ was confirmed by photoluminescence (PL) spectroscopy (Figure S7). This technic was demonstrated to be a powerful tool for assessing MOF purity, and specifically for identifying the presence of ZnO impurities in MOF samples, with the advantage of a higher sensitivity compared to powder XRD characterization.²¹ At ambient temperature, ZIF-8 exhibits a luminescence at 434 nm upon excitation at 335 nm, could be attributed to the $\pi^*-\pi$ transition of the 2-methylimidazolate

linkers.²² After the reduction process using NaBH₄, the emission spectrum of ZIF-8 displays an additional broad PL emission peak centered on 516 nm, strongly suggesting the presence of nanoscale ZnO particles. It is indeed known that the photoluminescence of ZnO nanoparticles show an emission peak at approximately 500 nm upon excitation at 350 nm as a result of the presence of defects (oxygen vacancies) on ZnO surface. This surface-related emission is particularly intense for ZnO particles with high surface-to-volume.²³ To summarize, reduction of copper cations with an aqueous solution of NaBH₄ results in their migration towards the outside of the MOF crystals, where the formation of the copper nanoparticles takes place. It is accompanied with the formation of ZnO nanocrystallites as impurities. The presence of such nanoscale semiconductor impurities in ZIF-8 sample should be avoided as their intrinsic physico-chemical properties²⁴ may interfere with the targeted applications of the ZIF-based materials.

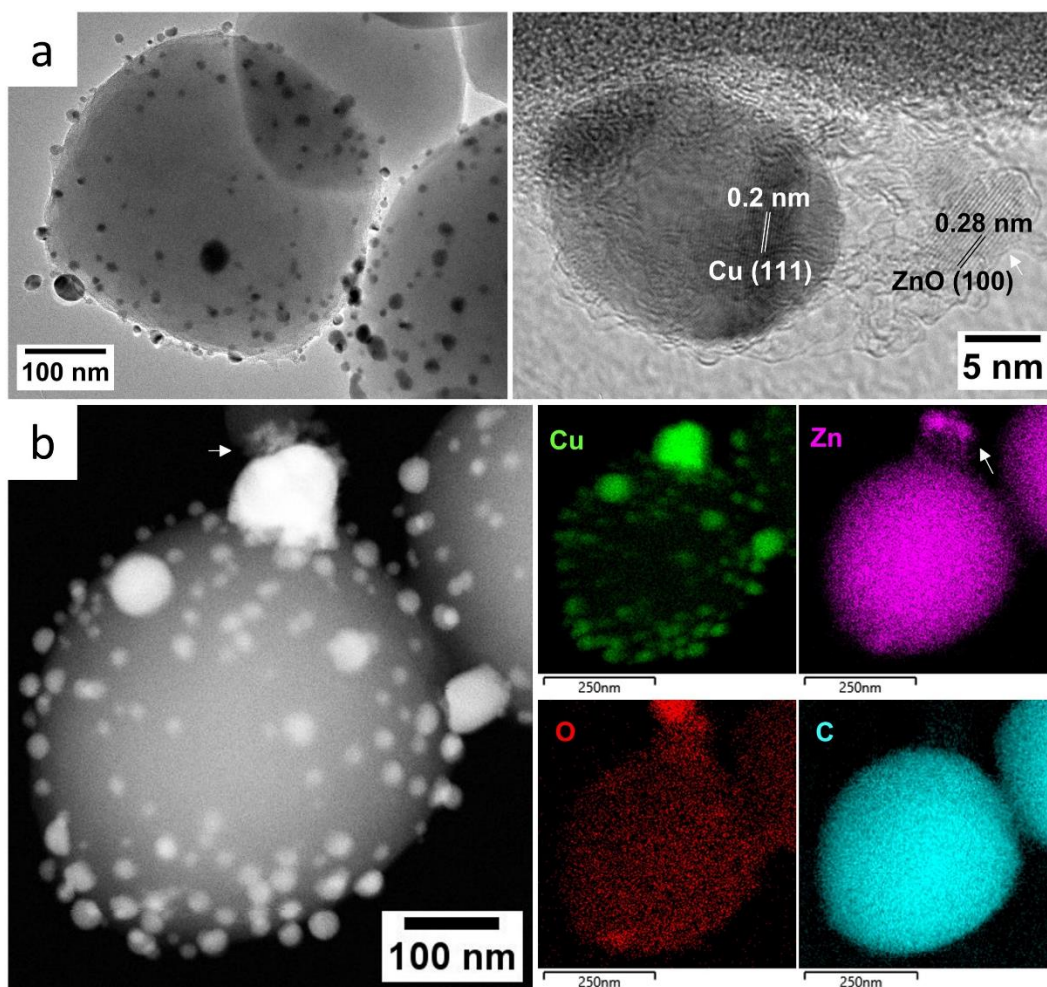


Figure 3. (a) TEM (left) and HRTEM (right) images, (b) HAADF image and corresponding Cu, Zn, O and C EDX element mapping of Cu/ZIF-8(NaBH₄). The white arrows indicate where are located the ZnO nanocrystallite aggregates.

The morphology of Cu/ZIF-8(H₂) is drastically different from that observed with Cu/ZIF-8(NaBH₄). Conventional TEM images of this sample show well-dispersed nanoparticles with a mean size of 22 nm mostly located within the bulk of ZIF-8 crystal (Figure 4a, a size histogram and additional HRTEM images are available in Figure S2b and S8, respectively). The chemical composition of the nanoparticles is confirmed by the lattice fringes with interplanar spacings of 0.20 corresponding to the (111) planes of metal copper (JCPDS 04-0836) observed on

nanoparticles by HRTEM (Figure 4a). The HAADF image and the corresponding element mapping also confirm the chemical composition of the nanoparticles and their dispersal within MOF (Figure 4b). Contrary to NaBH_4 , H_2 used as reduction agent under the experimental conditions used in this study does not trigger the formation of ZnO impurities. Indeed, ZnO impurities were indeed not detected on Cu/ZIF-8(H_2) by HRTEM analysis. In addition, the photoluminescence spectrum of H_2 -treated ZIF-8 did not displays any additional PL emission peak at approximately 500 nm upon excitation at 335 nm (Figure S7). These analyses therefore show that H_2 reduction (i) promotes the formation of copper nanoparticles mostly located within the bulk of the ZIF-8 crystals (i) does not lead to the formation of any ZnO nanoparticles.

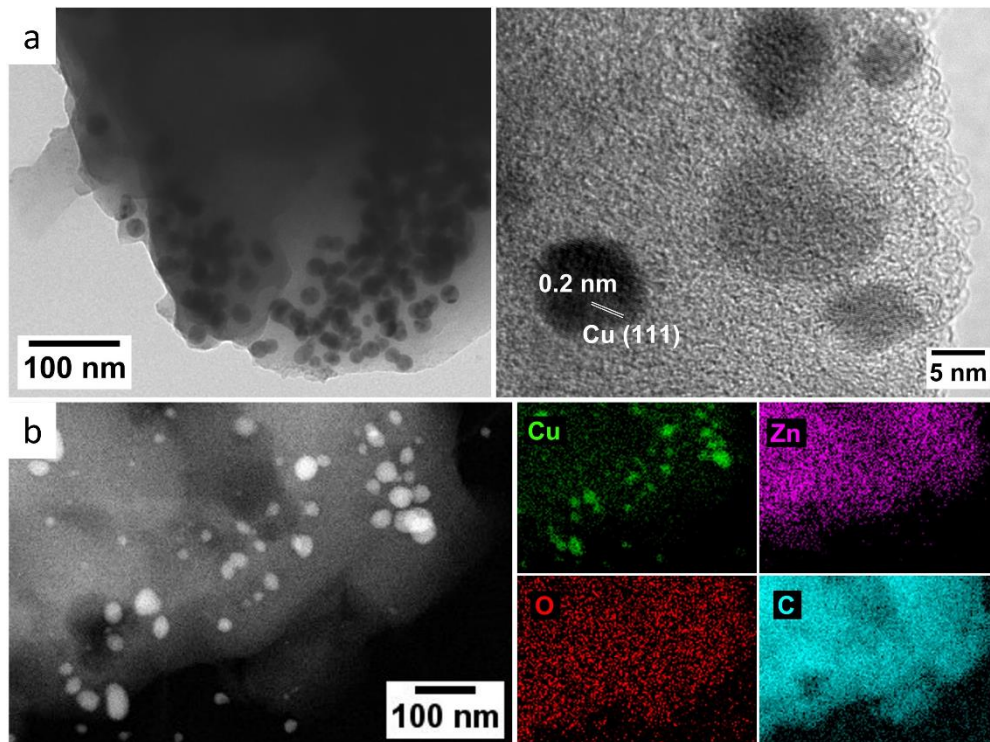


Figure 4. (a) TEM and HRTEM images and (b) HAADF image and corresponding Cu, Zn, O and C EDX element mappings of Cu/ZIF-8(H_2).

However, determining the location of copper nanoparticles, either within the bulk or onto the external surface of ZIF-8 crystals, is a difficult issue to address by the observation of two-dimensional TEM or STEM images alone. Therefore herein, the nanoparticles location depending on the reduction method was further investigated using X-ray photoelectron spectroscopy (XPS) analysis.

Table 2. Atomic percentages of the N, Zn and Cu elements in Cu/ZIF-8(H₂) and Cu/ZIF-8(NaBH₄)

	N _{1s}	Zn _{2p}	Cu _{2p}	O _{1s}	Cu _{2p} /N _{1s}	Cu _{2p} signal	
						Cu(II)	Cu(0) or Cu(I)
ZIF-8	20.7	7.4	-	4.34	-		
Cu/ZIF-8(H ₂)	19.1	4.2	0.8	7.47	0.19	77	23
Cu/ZIF-8(NaBH ₄)	15.8	2.9	2.4	12.76	0.83	7	93

Firstly, the chemical state analysis of Cu/ZIF-8(H₂) and Cu/ZIF-8(NaBH₄) NPs was performed. The main peaks in the survey spectra were assigned to C 1s, Cu 2p, O 1s, N 1s and Zn 2p (see Table 2 and Figure 5 (a) and (c)).

Theoretically, Cu 2p XPS signal is composed of two contributions, namely Cu 2p_{1/2} and Cu 2p_{3/2}, with a relative peak intensity of 1/2 and a binding energy (BE) difference of 20 eV (Figure S9). As expected, the positions of the Cu 2p_{1/2} and Cu 2p_{3/2} signals were found here at 953 eV and 933 eV, respectively, for Cu/ZIF-8(H₂) with a relative intensity of 0.47 and at 954.3 eV and 934.6 eV for Cu/ZIF-8(NaBH₄) with a relative intensity of 0.45. One obvious difference when comparing the signals of Cu/ZIF-8(H₂) to those of Cu/ZIF-8(NaBH₄) signals is that their ratios between the atomic percentages of Cu 2p and N 1s (Cu_{2p}/N_{1s}, in Table 2) are very different, namely 0.19 and 0.83, respectively (for similar copper contents close to 22 %, as quantified from ICP-OES

measurements). Such a result is an indication that Cu nanoparticles in Cu/ZIF-8(NaBH₄) are more preferentially located on the surface of the ZIF-8 crystals compared to the Cu/ZIF-8(H₂) solid.

As an attempt towards an in-depth analysis of the copper speciation, the Cu 2p_{3/2} signal of Cu NPs was fitted using CasaXPS software. The main peak at around 933 eV was separated into two contributions, the lower one being assigned to Cu(0) and/or Cu₂O (cuprous oxide, Cu(I)) species around 933 eV,²⁵ while at higher BE, 935.2 (±0.1) eV was assigned to divalent Cu(II), whose speciation could be Cu(OH)₂ (copper hydroxide) and/or CuO (cupric oxide) (Figure 5(b) and d). Such a signal decomposition clearly shows that the Cu/ZIF-8(NaBH₄) sample contains much more Cu(II) species than Cu(0) or Cu(I) species compared to the Cu/ZIF-8(H₂). Also, both the peak shape and the main peak to shake-up peak separation of Cu 2p_{3/2} signal of Cu/ZIF-8(NaBH₄) sample indicate that the speciation of Cu(II) compound is likely to be Cu(OH)₂. However, this could not be confirmed by a check of the O 1s signal. The corresponding peak around 531.7 (±0.1) eV has a full width at half maximum that could allow a deconvolution into several contributions, but the total O 1s intensity is too high to account only for oxidized copper species. This excess of oxygen may be explained by the contamination of the samples, as often observed in XPS spectra of real-world solids. More, inspection of the C 1s spectrum, as well as the C 1s/N 1s atomic percentage ratio, which is higher than that expected for ZIF-8, confirms that significant oxygen containing carbon species are present in the solids. Notably, the formation of the ZnO particles on the surface of ZIF-8 after Cu(II) reduction as observed on the TEM images (Figure 3) should also result in an excess of oxygen. As suggested by Marck Biesinger, the quantification of the relative [Cu(0) + Cu(I)] and Cu(II) species contents on a sample surface can be calculated from the main emission line of Cu 2p_{3/2} and the shake-up satellite intensity knowing the main peak/shake-up satellite peak areas for the pure corresponding Cu(II) sample.²⁵ Here, it can be assumed that the

partial oxidation of the Cu(0) NPs surface in both Cu/ZIF-8(H₂) and Cu/ZIF-8(NaBH₄) is likely to occur after the reduction step when the samples are stored in contact with ambient O₂ and H₂O. In this scenario, adsorbed water molecules dissociate and form surface hydroxyls groups resulting in a thin layer of mainly Cu(OH)₂ on the nanoparticle surface. Consequently, assuming that the oxidized copper species evidenced on CuZIF-8 surface are mainly formed of copper hydroxide, whose main peak/shake-up satellite peak area is 1.57, the percentage of Cu(II) on the Cu NP surface could be quantified to 10 % and 93 % for Cu/ZIF-8(H₂) and Cu/ZIF-8(NaBH₄), respectively, in line with the assumption that Cu NPs are more readily oxidized when located on the surface of ZIF-8 crystals like in the case of Cu/ZIF-8(NaBH₄). Notably, the different conditions used to synthesize the Cu NPs may also explain these differences of surface oxidation extent. Indeed, the wet reduction process achieved in the aqueous solution of NaBH₄ is expected to be more favorable to the oxidation of Cu NP than the dry process under gaseous dihydrogen flow.

Overall, the above results (TEM and XPS analyses) evidence that Cu NPs are more deeply embedded inside ZIF-8 crystals for Cu/ZIF-8(H₂) than in case of Cu/ZIF-8(NaBH₄). To explain this trend, we speculate that the wet conditions provided by the aqueous NaBH₄ solution, all the more that it is achieved under vigorous stirring conditions, favors the outward diffusion of cupric cations adsorbed within the ZIF-8 pores, leading to the formation of Cu⁰ NPs on the external surface of the crystals. Such an assumption is in line with the significant increase of the porous volume and BET surface area observed by N₂ sorption analysis after reduction, which become close to that of the parent ZIF-8 (Figure 2 and Table 1). Conversely, the dry gaseous condition inherent to the use of H₂ promotes the fast reduction of cupric cations localized within the ZIF-8 porosity after the impregnation process, leading to the growth of copper NPs mostly positioned within the pores.

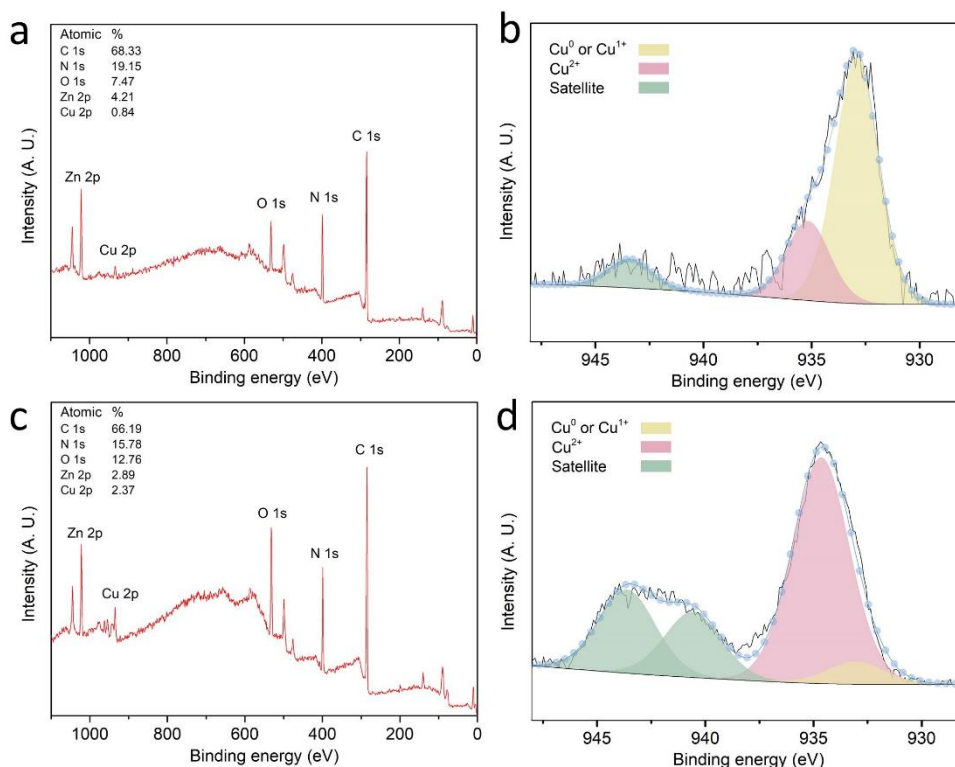


Figure 5. Full XPS spectra (a and c) and high-resolution XPS spectra of Cu 2p_{3/2} (b and d) of Cu/ZIF-8(H₂) (a and b) and of Cu/ZIF-8(NaBH₄) (c and d).

3.2 Catalytic activity and heterogeneity test: effect of the reduction method.

Oxidation of benzyl alcohol in air. Selective oxidation of benzyl alcohol was selected as model reaction to monitor and compare the catalytic activity of Cu/ZIF-8(H₂) and Cu/ZIF-8(NaBH₄) as well as for optimizing the reaction conditions.

Reactions were performed in the presence of TEMPO and DMAP. TEMPO is a free radical that is classically used in the aerobic oxidation of alcohols, while DMAP mainly acts as an organic base co-catalyst. Reactions were performed in acetonitrile as a solvent, at 60 °C during 24h in the presence of air as an oxidation agent. The conversion extent of benzyl alcohol and the benzaldehyde yield are shown in Table 3.

Table 3. catalytic oxidation of benzyl alcohol

Catalysts	Time (h)	Conversion (%)	Yield benzaldehyde (%)
ZIF-8	24	-	-
Cu/ZIF-8(NaBH ₄)	24	61	58
Cu/ZIF-8(H ₂)	24	62	66

Test conditions: 5 mg catalyst (10 mol %), 5 mM TEMPO, 100 mM benzyl alcohol, 1 atm of air, 2 mL acetonitrile, 70 °C and during 24h.

The control experiment using pure ZIF-8 did not yield any benzaldehyde formation after 24 h of reaction at 70 °C. In contrast, using Cu/ZIF-8(H₂) and Cu/ZIF-8(NaBH₄) as catalysts led to benzyl alcohol conversions of 62 % and 61%, respectively (benzaldehyde yields reach 66 % and 58 % after 24h with Cu/ZIF-8(H₂) and Cu/ZIF-8(NaBH₄), respectively). These results demonstrate the critical role of copper as a catalyst. No benzylic acid was detected, indicating that no overoxidation reaction occurs. Notably, Figure 6 shows that the kinetic profiles of the first 6 hours of reaction catalyzed with Cu/ZIF-8(H₂) and Cu/ZIF-8(NaBH₄) are different. Indeed, using Cu/ZIF-8(H₂) induces a lag time of 3 h, presumably due to some diffusional limitations of the alcohol inside the pores of ZIF-8 whose size (from 3.4 Å for the pristine ZIF-8 to 6.9 Å for its open form²⁶) is close to that of benzyl alcohol (molecular length ca. 7.9 Å, width ca. 5.3 Å²⁷), thus slowing down benzyl alcohol diffusion towards copper nanoparticles trapped within the bulk ZIF-8 crystals. Conversely, when using Cu/ZIF-8(NaBH₄) as a catalyst, benzaldehyde yield increases almost linearly with the reaction time. In this case, because the nanoparticles are likely located on the surface of the ZIF-8 crystals, they are directly accessible to the reactant, so that there is no diffusional barrier to overcome. The difference between reaction kinetics when comparing the two catalysts is even

more significant when a bulkier substrate is employed instead of benzyl alcohol. Indeed, for the 3,5-di-tert-butyl-4-hydroxybenzyl alcohol, a bulky derivative of benzyl alcohol, the oxidation yield of the corresponding aldehyde after 2h of reaction remains below 10 % with Cu/ZIF-8(H₂) while a benzaldehyde yield of 43 % is obtained with Cu/ZIF-8(NaBH₄) after the same reaction time. Cu/ZIF-8(H₂) therefore fully takes advantage of the sieving effect of ZIF-8. Indirectly, these results confirm the effect of the copper reduction procedure on the location of the Cu NPs: the thermal treatment under H₂ flow promotes the Cu⁰ nanoparticle growth within the bulk of ZIF-8 crystals, which promotes a size selectivity relative to the oxidation substrate.

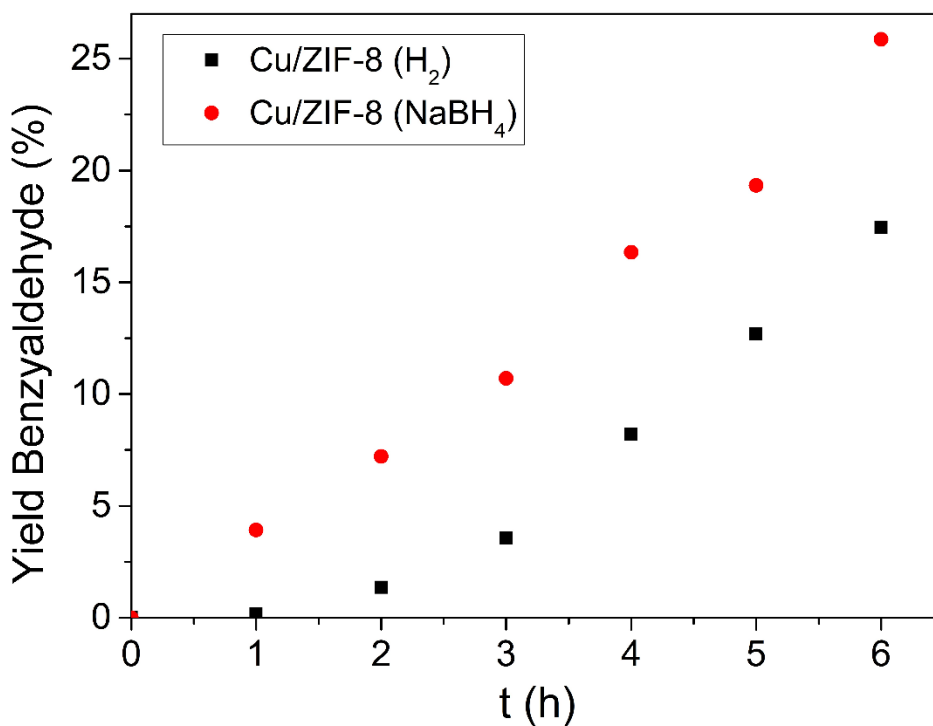


Figure 6. Kinetic profiles of the benzaldehyde reaction catalyzed with Cu/ZIF-8(NaBH₄) and Cu/ZIF-8(H₂). Reaction conditions: 5 mg catalyst (10 mol %), 5 mM TEMPO, 100 mM benzyl alcohol, 1 atm of air, 2 mL acetonitrile, and 60 °C.

The stability and the heterogeneous character of the two catalysts Cu/ZIF-8(H₂) and Cu/ZIF-8(NaBH₄) were then monitored and compared. Cu/ZIF-8(H₂) and Cu/ZIF-8(NaBH₄) catalysts were removed from the hot reaction medium by means of filtration using a 0.45 μm filtration membrane after 5 h and 3 h of reaction, respectively, and the catalytic activity of the filtrate for benzyl alcohol oxidation was further monitored (Figure 7).

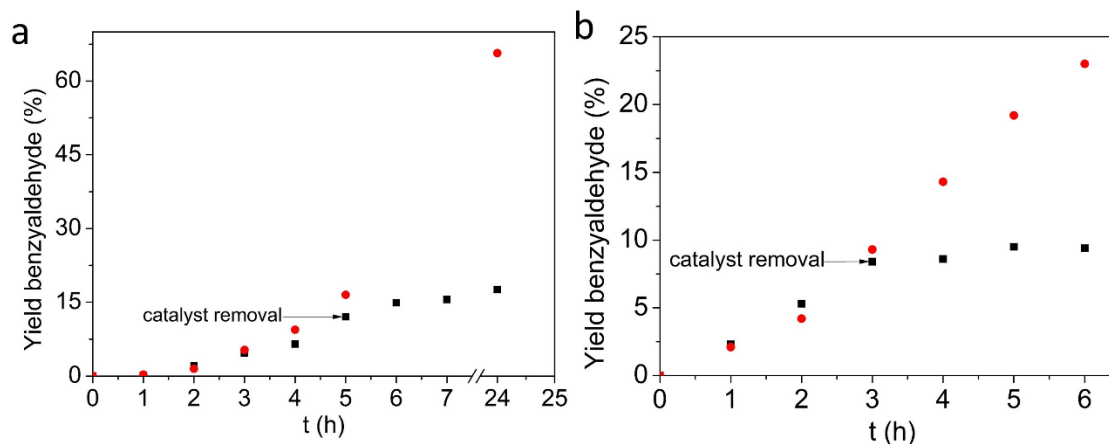


Figure 7. Assessment of heterogeneous catalysis: a) Cu/ZIF-8(H₂) was removed after 5 h of reaction, b) Cu/ZIF-8(NaBH₄) was removed after 3 h of reaction. Reaction conditions: 5 mg catalyst (10 mol %), 5 mM TEMPO, 100 mM benzyl alcohol, 1 atm of air, 2 mL acetonitrile, and 60 °C.

The absence of reaction in the reaction mixture after the catalyst removal with both catalysts indicates the absence of active sites leaching during the reaction course. This result points out the fully heterogeneous character of both Cu/ZIF-8(H₂) and Cu/ZIF-8(NaBH₄) catalysts. The recyclability of the two types of catalysts was also evaluated and compared by reusing the catalysts five times subsequently. The catalysts were removed by centrifugation between two consecutive tests and thoroughly washed with acetonitrile. Figure 8 shows the benzaldehyde yield plotted as a function of time for each type of catalyst during the first 5 h of reaction. Similar benzaldehyde

yields were obtained for the first four cycles with Cu/ZIF-8(H₂) indicating the excellent stability of this catalyst (Figure 8a). In contrast, benzaldehyde yield decreases after each cycle with Cu/ZIF-8(NaBH₄) (Figure 8b). Elemental ICP-OES analyses of the two catalysts before and after the five consecutive cycles confirm the lower stability of Cu/ZIF-8(NaBH₄) compared to Cu/ZIF-8(H₂). Copper content in Cu/ZIF-8(NaBH₄) drops from 22 wt. % for the freshly synthesized material to 10 % after the fifth cycle. Such a decrease is not observed in the case of Cu/ZIF-8(H₂) for which the copper content remains almost stable, decreasing only slightly from 22 wt. % for the fresh catalyst to 19 wt. % after 5 cycles. PXRD characterization of the catalysts after the fifth cycle also evidence the difference of stability of the two types of catalyst (Figure S10). While the intensities of the diffraction peaks assigned to ZIF-8 seemed not to be affected by the catalytic tests, the three diffraction peaks observed on the XRD profile of the fresh Cu/ZIF-8(NaBH₄) representing the (111), (200) and (220) planes of Cu⁰ (at 43.39°, 55.50° and 74.08°, respectively) almost completely disappeared after the five consecutive catalytic tests, corroborating the leaching of copper species as measured by ICP-OES analysis. In contrast, XRD peaks attributed to ZIF-8 and Cu⁰ in Cu/ZIF-8(H₂) diffraction pattern remain unchanged after cycling the catalyst, confirming its stability. Furthermore, the N₂ physisorption curves Cu/ZIF-8(NaBH₄) and Cu/ZIF-8(H₂) measured after cycling are similar to those of the freshly synthesized catalysts (Figure S11), which is also consistent with the putative location of copper NPs: when located on the Cu/ZIF-8(NaBH₄) external surface, their leaching has no influence on the textural properties of ZIF-8 whereas in case of Cu/ZIF-8(H₂) material, unchanged textural properties is in good accordance with the good stability of the catalyst. In this case, the hybrid ZIF-8 network entrapping Cu NPs efficiently stabilizes them and prevents copper species from leaching during both the reaction course and the separation/washing processes.

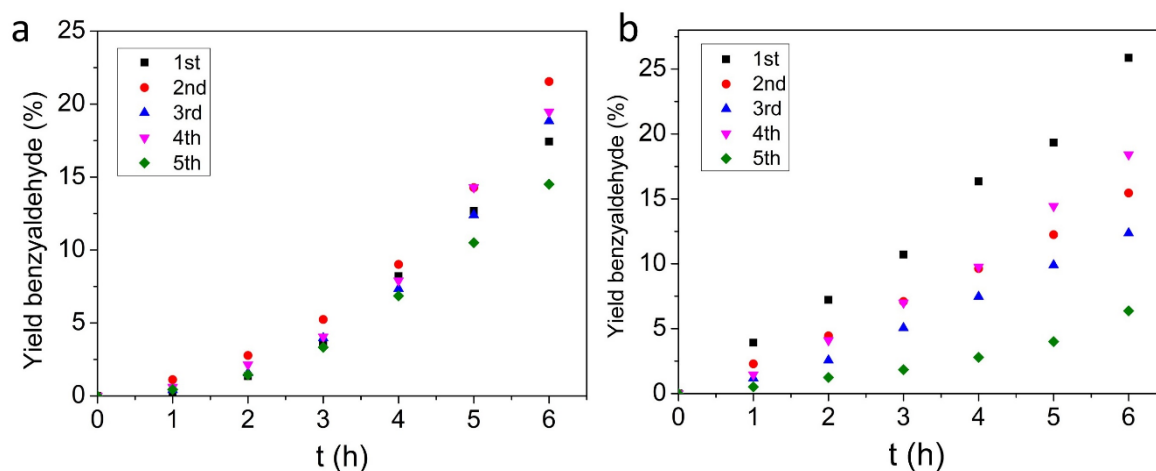
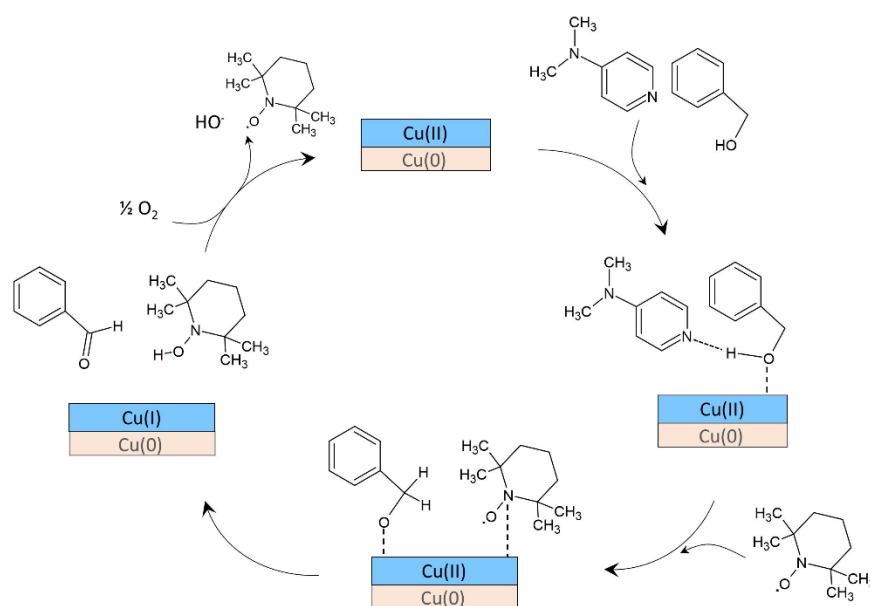


Figure 8. Recycling tests with a) Cu/ZIF-8(H₂) and b) Cu/ZIF-8(NaBH₄) as catalysts. Reaction conditions: 5 mg catalyst (10 mol %), 5 mM TEMPO, 100 mM benzyl alcohol, 1 atm of air, 2 mL acetonitrile, and 60 °C.

By trapping the Cu NPs within ZIF-8 bulk, this strategy hence allows for efficient heterogenization and recycling of Cu(II) sites, that are believed to be the active sites that catalyze the aerobic oxidation of alcohols in the presence of TEMPO. A mechanism for the oxidation of benzyl alcohol is proposed in the following, based on previous reports focused on the homogeneous catalysis of aerobic alcohol oxidation involving copper sites and TEMPO (scheme 2).⁵ As indicated by XPS analysis, the surface of the copper nanoparticles before catalysis test is decorated with copper(II) species (CuO and Cu(OH)₂). The alcohol is therefore first expected to coordinate to the surface copper(II) atoms, facilitating the deprotonation of the alcohol to form a Cu(II)-alkoxide. The alcohol deprotonation may be achieved either by vicinal copper hydroxide groups, the closest nitrogen atoms of the 2-methyl-imidazolate MOF linkers or the additional organic base DMAP. A minimum amount of DMAP was however shown to be necessary for the alcohol oxidation to proceed efficiently (Figure 9b), suggesting that this basic compound is the main responsible for the alcohol deprotonation. A hydrogen transfer from the α -carbon of the

alcohol to TEMPO, which is also coordinated to the surface copper(II) cations, then results in the formation of the carbonyl product and in the generation of surface copper(I) cations. The aerobic oxidation of both TEMPOH and surface copper(I) finally results in the regeneration of TEMPO and surface copper(II) cations, hence terminating the catalytic cycle. In this process, the critical role of TEMPO and O₂ was evidenced experimentally since they are mandatory for the reaction to proceed.

Scheme 2. Possible mechanism for the aerobic oxidation of benzyl alcohol catalyzed by Cu(II) sites on the surface of Cu/ZIF-8 Cooper nanoparticles with TEMPO as co-catalyst.



Cu/ZIF-8(H₂) is therefore the most promising of the two catalysts. Its activity was then studied as the function of different experimental parameters.

Optimization of the reaction condition with Cu/ZIF-8(H₂) as catalyst. The effect of the reaction temperature was first monitored. Figure 9a shows that the benzaldehyde yield determined after

24h of reaction increases from 51 % to 66 % with an increase of temperature from 50 °C to 70 °C. Benzaldehyde yield remains then constant when the temperature is further increased to 80 °C. Then, the reaction was conducted with four different DMAP to benzyl alcohol molar ratios. Figure 9b shows that benzyl alcohol takes place only above a DMAP to benzyl alcohol molar ratio of 0.05. The benzaldehyde yield obtained after 24h of reaction is indeed only 6% when the reaction is achieved without DMAP, while it reaches around 65 % for DMAP to benzyl alcohol molar ratio higher than 0.05. Hence, the copper-coordinated imidazolate linkers located close to the copper nanoparticles within the ZIF-8 framework do not provide sufficiently strong basic sites to deprotonate benzyl alcohol and favors the formation of the active Cu(II)-alkoxide intermediate necessary for the generation of benzaldehyde, as described by S. S. Stahl and collaborators.²⁸ The presence of a minimum amount of the strong organic base DMAP is therefore required.

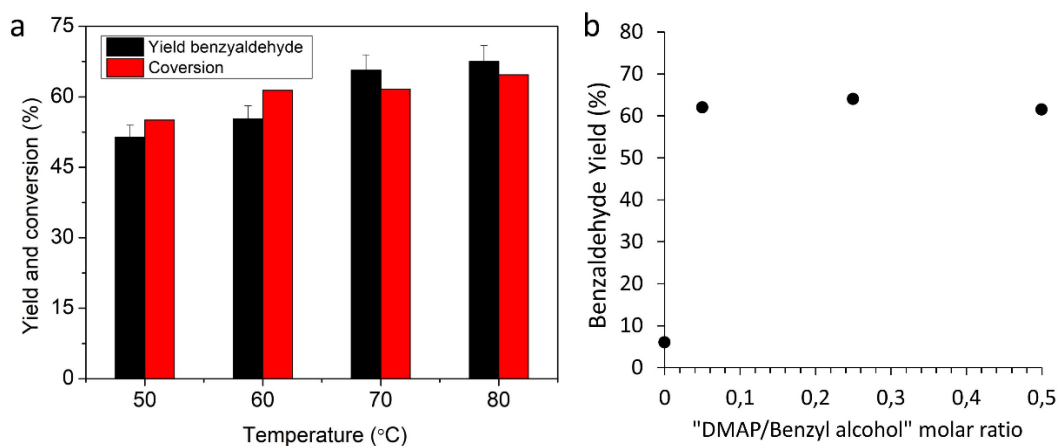


Figure 9. Cu/ZIF-8(H₂) activity as a function of (a) the reaction temperature and (b) the molar ratio between DMAP and benzyl alcohol. Reaction conditions: (a) 5 mg Cu/ZIF-8(H₂) (10 mol %), 5 mM TEMPO, 100 mM benzyl alcohol, 1 atm of air, 2 mL acetonitrile, 24 h (b) 5 mg Cu/ZIF-8(H₂) (10 mol %), 5 mM TEMPO, 100 mM benzyl alcohol, 1 atm of air, 2 mL acetonitrile, T = 70 °C, 24 h.

Table 4. Influence of solvent and oxygen source upon benzyl alcohol yield.

Solvent	Oxidant	Yield (%)	Conversion (%)
Water	O ₂	0	29
Ethanol	O ₂	3	10
Neat	O ₂	57	59
Acetonitrile	O ₂	78	77
Acetonitrile	Air	66	62

Reaction conditions: 5 mg Cu/ZIF-8(H₂) (10 mol %), 5 mM TEMPO, 100 mM benzyl alcohol, 1 atm of gas phase, 2 mL solvent (when used), T = 70 °C, 24 h.

The reaction was also tested in different solvents (Table 4). Benzaldehyde yield was monitored as a function of time within three solvents: water, acetonitrile and ethanol or without any solvent. The highest activity of Cu/ZIF-8(H₂) is obtained in acetonitrile, with a benzaldehyde yield of 78 % (Selectivity > 99%). Ethanol and water however do not allow the production of benzaldehyde. The reaction carried out without additional solvent, where benzaldehyde is used both as substrate and solvent, leads to a yield equal to 57%. The catalyst is however degraded during the reaction, which is mainly catalyzed under homogeneous conditions.

Finally, pure O₂ was compared to air as green and cheap source of oxygen (Table 4). When employing molecular O₂, Cu/ZIF-8(H₂) showed only a 15% higher benzyl alcohol conversion (77%) than with air and a similarly high yield (78 % compared to 66%, respectively). Using air instead of pure O₂ therefore does not significantly penalize the catalysis performances of Cu/ZIF-8(H₂), which are still satisfying.

Based on these results, the best reaction conditions for benzyl alcohol oxidation, considering both reaction efficiency and sustainability, are the following: in acetonitrile as solvent, at a temperature T = 70°C, with a molar ratio DMAP to benzyl alcohol equal to 0.05 and using air as

sustainable oxygen source. Cu/ZIF-8(H₂) therefore provides a new heterogeneous and recyclable system allowing for the aerobic oxidation of benzyl alcohol. Its performances are comparable to those of other heterogeneous copper-based systems catalyzing alcohol oxidation with TEMPO as co-catalyst and O₂ as oxidant reported in the literature. However, compared to these catalysts, Cu/ZIF-8(H₂) combined several advantages: it does not require the chemical modification of the support surface or the use of expensive organic linkers, it is stable, and works under relatively mild temperature and using atmospheric air as oxygen source instead of pure O₂ (Table S1). Moreover, this catalytic system integrates different reactive sites (the N-sites of the ZIF-8 organic linkers) making possible its use for tandem catalysis. The optimal reaction conditions were hence used to set the stepwise benzyl alcohol oxidation and Knoevenagel condensation described in the next section.

Stepwise benzyl alcohol oxidation and Knoevenagel condensation. The catalytic behavior of Cu/ZIF-8(H₂) was investigated in a stepwise process coupling benzyl alcohol oxidation with the Knoevenagel reaction, an important C–C coupling reaction widely used in the synthesis of fine chemicals (Scheme 3).²⁹ This “one-pot” process is expected to enhance the sustainability of the synthesis of benzylidene malononitrile, a highly valuable molecule regarding its role as molecular building block for the construction of various nitrogenous heterocycles with versatile biological activities.^{30,31}

The rationale for this approach relies on the fact that, in addition to the Cu sites responsible for the alcohol oxidation, the Cu/ZIF-8(H₂)/TEMPO/DMA system also contains two types of chemical basic sites that were recently reported to efficiently catalyze the Knoevenagel reaction: (i) the basic N-moieties of the ZIF-8 framework³² and (ii) DMAP.³³ Here, both ZIF-8 and DMAP

were first independently tested as catalysts for the Knoevenagel condensation of benzaldehyde with malononitrile under the optimized conditions of benzyl alcohol oxidation set before.

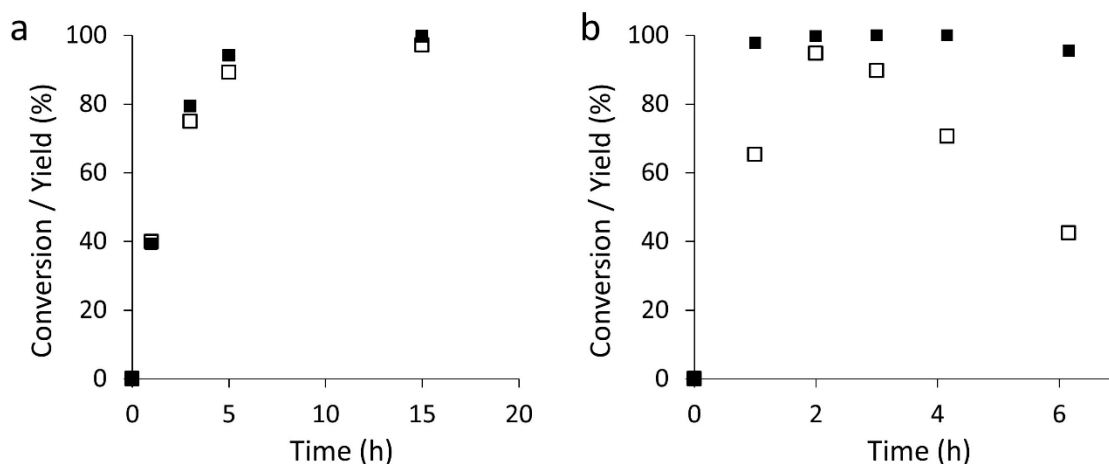


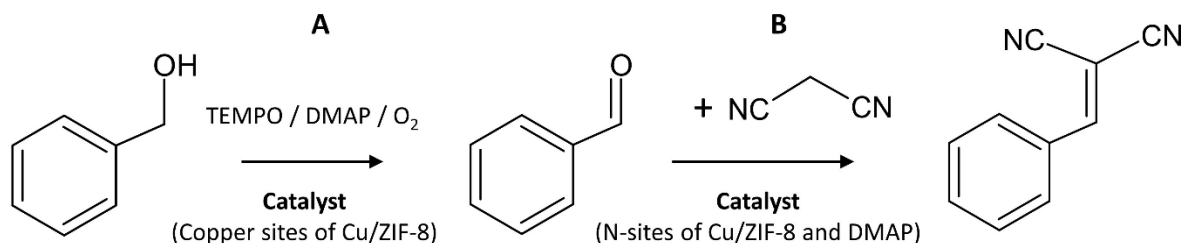
Figure 10. Activity of (a) ZIF-8 and (b) DMAP as catalysts for the Knoevenagel condensation of benzaldehyde with malononitrile. Filled squares correspond to the benzaldehyde conversion and empty squares represent the benzylidene malononitrile yield. Reaction conditions: (a) 5 mg ZIF-8, 190 mM malononitrile, 100 mM benzaldehyde, 2 mL acetonitrile and 70 °C, (b) 5.7 mM DMAP, 190 mM malononitrile, 100 mM benzaldehyde, 2 mL acetonitrile and 70 °C.

The use of ZIF-8 alone results in benzyl alcohol conversion and BIM yield higher than 95% after 5h of reaction (Figure 10a). With DMAP alone, benzyl alcohol is fully converted and the yield of BIM reaches 94% after 1h of reaction (Figure 10b). However, the yield of BIM decreases after reaching this maximum. We hypothesize that this drop is due to the reaction of BIM with malononitrile dimer to form polyfunctionality substituted benzenes and pyridine derivatives as side products. Both dimerization of malononitrile added as a two-fold excess compared to benzaldehyde and the reaction of the dimer with BIM were indeed shown to be achieved in basic media and at temperatures close to that used in this study.^{34,35} This decrease of BIM yield is

however not observed when ZIF-8 alone is used as catalyst, suggesting that ZIF-8 is selective towards the Knoevenagel reaction under the reaction conditions set in this study (Figure 10a).

The stepwise process coupling benzyl alcohol oxidation with the Knoevenagel reaction was then achieved with Cu/ZIF-8(H₂) as catalyst (Scheme 3).

Scheme 3. Reaction scheme displaying the stepwise reaction: (A) benzyl alcohol oxidation into benzaldehyde followed by (B) the Knoevenagel condensation of benzaldehyde with malononitrile to form the benzylidene malononitrile. The catalytic sites for the two reactions are indicated.



In a first attempt, all reagents involved in the two reactions were added at once into the reaction mixture in order to perform the tandem reaction in a one-step process. However, the combination did not allow for the oxidation of benzyl alcohol to occur. A similar result was reported by C. S. Hinde and collaborators who also studied the association of alcohol oxidation and subsequent Knoevenagel condensation but with a different catalytic system.³⁶ The deleterious effect of malononitrile over the oxidation of benzyl alcohol during the alcohol oxidation step is probably due to the poisoning of the copper nanoparticle surface. Alternatively, malononitrile was therefore added only after completion of the benzyl oxidation step (at $t = 26\text{h}$). Resulting yields of benzyl alcohol, benzaldehyde and benzylidene malononitrile as a function of time are shown in Figure 11.

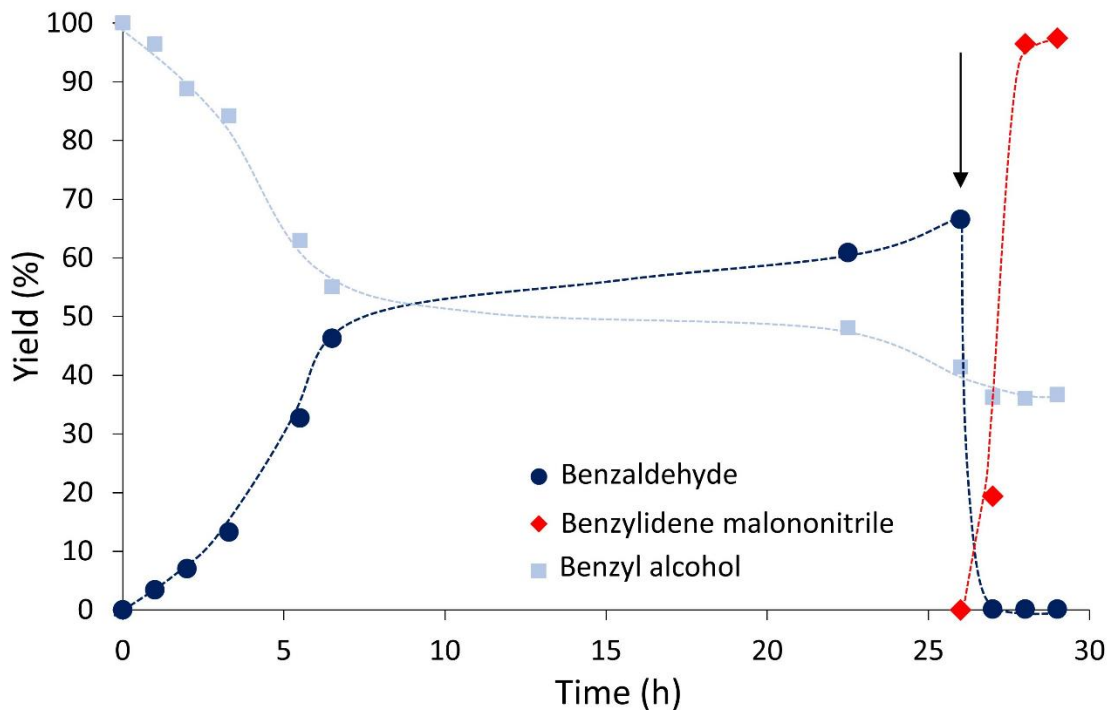


Figure 11. Time course for the one-pot tandem reaction. Malononitrile was added after 26h of benzyl alcohol oxidation (indicated by the arrow). Colored dotted lines were drawn to guide the eyes. Reaction conditions : 5 mg Cu/ZIF-8(H₂), 5 mM TEMPO, 100 mM benzyl alcohol, 5.7 mM DMAP, 190 mM malononitrile, 1 atm of air, 2 mL acetonitrile and 70 °C.

A benzaldehyde yield of 65% is reached after 26h. Then the addition of malononitrile to the reaction mixture leads to the consumption of benzaldehyde that occurs concomitantly to the production of benzylidene malononitrile. The latter product is obtained with a yield higher than 95% relative to benzaldehyde after only 2h of reaction that is a yield equal to 65 % when it is calculated based on the benzyl alcohol. The same tandem reaction was achieved without DMAP. The yield of benzaldehyde then reaches 16% after 66 h and the yield of benzylidene malononitrile is 5% after addition of the malononitrile based on the benzyl alcohol quantity introduced at the start of the reaction. This result confirms the critical role of DMAP in the catalysis of benzyl alcohol oxidation (Figure 9b).

Conclusion. Surface oxidized-Cu⁰ nanoparticles supported on ZIF-8 crystals with a significant activity towards the oxidation of benzyl alcohol were synthesized by the impregnation of ZIF-8 with a copper precursor followed by the reduction of Cu²⁺ into Cu⁰ nanoparticles. The oxidation of the nanoparticle surface then occurs during the storage of the catalysts under ambient conditions. Two procedures were followed and compared for the reduction of the Cu²⁺ cations into Cu⁰: (i) a dried treatment at high temperature under H₂ flow and (ii) a wet treatment in an aqueous solution of NaBH₄. Only the dry reduction procedure under H₂ atmosphere allowed for the synthesis of well-dispersed Cu⁰ nanoparticles located within the bulk of the ZIF-8 crystals. The entrapment of the copper nanoparticles within the microporous hybrid network confers to the catalysts (Cu/ZIF-8(H₂)) a high stability and a potential for selective catalysis based on the molecular size of the substrates. In contrast, the use of NaBH₄ leads to the formation of copper nanoparticles exclusively located on the external surface of the ZIF-8 crystals. It is noteworthy that copper nanoparticles were observed along with ZnO impurities generated by the partial degradation of the MOF during the NaBH₄ treatment. The resulting catalyst Cu/ZIF-8(NaBH₄) presents a lower stability than Cu/ZIF-8(H₂). To our knowledge, the effect of the procedure of metal precursor reduction over (i) the location of the final metal nanoparticles on MOF and (ii) the purity of the sample was not reported yet. Finally, the most stable and pure catalyst (Cu/ZIF-8(H₂)) was successfully applied to implement a *one-pot* cascade chemical process where the benzyl alcohol oxidation into benzaldehyde is subsequently transformed into benzylidene molononitrile by a Knoevenagel condensation step catalyzed by both DMAP and the basic imidazolate linkers of the ZIF-8 framework.

AUTHOR INFORMATION

Corresponding Authors:

julien.reboul@sorbonne-universite.fr

claire.jolivald@sorbonne-universite.fr

Author Contributions

The manuscript was written through contributions of all authors. All authors have given approval to the final version of the manuscript.

Funding Sources

The work was funded by the doctoral school ED 397 of Sorbonne University

Supporting Information

The H₂-TPR analysis of Cu²⁺/ZIF-8; the size histograms of Cu nanoparticles in Cu/ZIF-8(NaBH₄) and Cu/ZIF-8(H₂) ; additional HRTEM images of Cu/ZIF-8(NaBH₄) ; TEM and HRTEM images as well as HAADF image and corresponding Cu, Zn, O and C EDX element mappings of Cu/ZIF-8(NaBH₄); local atomic composition analyses of the ZnO nanoparticles in Cu/ZIF-8(NaBH₄) ; HTEM images and PXRD analyses of ZIF-8 crystals dispersed in water without NaBH₄ and in an aqueous solution of NaBH₄ ; additional TEM images of copper nanoparticles in Cu/ZIF-8(H₂) ; XPS signals on Cu 2p BE range and the calculation used to quantify Cu(II) on the copper nanoparticle surface ; Comparison of XRD patterns and N₂ adsorption isotherms of Cu/ZIF-8(NaBH₄) and Cu/ZIF-8(H₂) before and after 5 catalysis cycles; a table comparing the different

supported *copper*-based catalysts (supported single sites and copper nanoparticles) used for the *aerobic* oxidation of benzyl alcohol reported in the literature with Cu/ZIF-8(H₂).

ACKNOWLEDGMENT

The authors thank the Ministère de l'Enseignement Supérieur, de la Recherche et de l'Innovation for providing the financial support for the work of M. Yifan Zan. This work was supported by Sorbonne Université, Centre National de la Recherche Scientifique (CNRS) and Région Ile de France.

REFERENCES

- [1] Arends, I.W.C.E.; Sheldon, R.A. *Modern Oxidation Methods*, 2nd ed.; Backvall, J.-E., Ed.; Wiley VCH: Weinheim, Germany, 2010.
- [2] Ferraz, C. P.; Garcia, M. A. S.; Teixeira-Neto, E.; Rossi, L. M. Oxidation of Benzyl Alcohol Catalyzed by Gold Nanoparticles Under Alkaline Conditions: Weak vs. Strong Bases. *RSC Adv.* **2016**, 6, 25279-25285. DOI: 10.1039/C6RA01795A
- [3] Durdell, L. J.; Cucuzzella, C.; Parlett, C. M. A.; Isaacs, M. A.; Wilson, K.; Lee A. F. Platinum Catalysed Aerobic Selective Oxidation of Cinnamaldehyde to Cinnamic Acid. *Catal. Today* **2019**, 333, 161-168. DOI: 10.1016/j.cattod.2018.02.052
- [4] Silva, T. F. S.; Martins L. M. D. R. S. Recent Advances in Copper Catalyzed Alcohol Oxidation in Homogeneous Medium. *Molecules* **2020**, 25 (3), 748-762. DOI: 10.3390/molecules25030748

[5] Ryland, B. L.; Stahl S. S. Practical Aerobic Oxidations of Alcohols and Amines with Homogeneous Copper/TEMPO and Related Catalyst Systems. *Angew. Chem. Int. Ed.* **2014**, 53 (34), 8824-8838. DOI: 10.1002/anie.201403110

[6] Silva, T. F. S.; Martins, L. M. D. R. S. Recent Advances in Copper Catalyzed Alcohol Oxidation in Homogeneous Medium. *Molecules* **2020**, 25, 748-762. DOI: 10.3390/molecules25030748

[7] Xu, B.; Senthilkumar, S.; Zhong, W.; Shen, Z.; Lu, C.; Liu X. Magnetic Core–Shell Fe₃O₄@Cu₂O and Fe₃O₄@Cu₂O–Cu Materials as Catalysts for Aerobic Oxidation of Benzylic Alcohols Assisted by TEMPO and N-methylimidazole. *RSC Adv.* **2020**, 10, 26142-26150. DOI: 10.1039/D0RA04064A

[8] Ibrahem, I.; Iqbal, M. N.; Verho, O.; Eivazihollagh, A.; Olsén, P.; Edlund, H.; Tai, C.-W.; Norgren, M.; Johnston, E. V. Copper Nanoparticles on Controlled Pore Glass and TEMPO for the Aerobic Oxidation of Alcohols. *ChemNanoMat* **2018**, 4, 71-75. DOI: 10.1002/cnma.201700309

[9] Buxaderas, E.; Graziano-Mayer, M.; Volpe, M. A.; Radivoy, G. Bimetallic Cu-Pd Nanoparticles Supported on Bio-silica as an Efficient Catalyst for Selective Aerobic Oxidation of Benzylic Alcohols. *Synthesis* **2017**, 49, 1387-1393. DOI: 10.1055/s-0036-1588628

[10] Ju, S.; Yusuf, M.; Jang, S.; Kang, H.; Kim, S.; Park, K. H. Simple Transformation of Hierarchical Hollow Structures by Reduction of Metal–Organic Frameworks and Their Catalytic Activity in the Oxidation of Benzyl Alcohol. *Chem. Eur. J.* **2019**, 25, 7852-7859. DOI: 10.1002/chem.201900231

[11] Zhang, K.; Shang, H.; Li, B.; Wang, Z.; Lu, Y.; Wang, X. Structural Design of Metal Catalysts Based on ZIFs: From Nanoscale to Atomic Level. *Nano Select* **2021**, *2*, 1902-1925. DOI: 10.1002/nano.202100009

[12] Wang, W.; Chen, S.; Guisasola Cal, E.; Martínez Moro, M.; Moya, S.; Coy, E.; Wang, C.; Hamon, J.-R.; Astruc, D. ZIF-8-based vs. ZIF-8-Derived Au and Pd Nanoparticles as Efficient Catalysts for the Ullmann Homocoupling reaction. *Inorg. Chem. Front.* **2020**, *7*, 3945-3952. DOI: 10.1039/D0QI00831A

[13] Kamaraj, K.; Kim, E.; Galliker, B.; Zakharov, L. N.; Rheingold, A. L.; Zuberbühler, A. D.; Karlin K. D. Copper(I) and Copper(II) Complexes Possessing Cross-Linked Imidazole-Phenol Ligands: Structures and Dioxygen Reactivity. *J. Am. Chem. Soc.* **2003**, *125* (20), 6028-6029. DOI: 10.1021/ja034263f

[14] Abdelhamid, H. N. A Review on Hydrogen Generation from the Hydrolysis of Sodium Borohydride. *Int. J. Hydrog. Energy* **2021**, *46* (1), 726-765. DOI: 10.1016/j.ijhydene.2020.09.186

[15] Zhou, Y.-H.; Cao, X.; Ning, J.; Ji, C.; Cheng, Y.; Gu, J. Pd-Doped Cu Nanoparticles Confined by ZIF-67@ZIF-8 for Efficient Dehydrogenation of Ammonia Borane. *Int. J. Hydrog. Energy* **2020**, *45* (56), 31440-31451. DOI: 10.1016/j.ijhydene.2020.08.141

[16] Lv, X.-W.; Wang, L.; Wang, G.; Hao, R.; Ren, J.-T.; Liu, X.; Duchesne, P. N.; Liu, Y.; Li, W.; Yuan, Z.-Y.; Ozin, G. A. ZIF-supported AuCu Nanoalloy for Ammonia Electrosynthesis from Nitrogen and Thin Air. *J. Mater. Chem. A* **2020**, *8*, 8868-8874. DOI: 10.1039/D0TA02832K

[17] Guo, C.; Liang, C.; Qin, X.; Gu, Y.; Gao, P.; Shao, M.; Wong, W.-T. Zeolitic Imidazolate Framework Cores Decorated with Pd Nanoparticles and Coated Further with Metal–Organic

Framework Shells (ZIF-8@Pd@MOF-74) as Nanocatalysts for Chemoselective Hydrogenation Reactions. *ACS Appl. Nano Mater.* **2020**, 3 (7), 7242-7251. DOI: 10.1021/acsanm.0c01566

[18] Feng, Y.; Yan, G.; Wang, T.; Jia, W.; Zeng, X.; Sperry, J.; Sun, Y.; Tang, X.; Lei, T.; Lin, L. Cu¹-Cu⁰ Bicomponent CuNPs@ZIF-8 for Highly Selective Hydrogenation of Biomass Derived 5-Hydroxymethylfurfural. *Green Chem.*, **2019**, 21, 4319-4323. DOI: 10.1039/C9GC01331H

[19] Tuan, D. D.; Lin, K.-Y. A. Ruthenium Supported on ZIF-67 as an Enhanced Catalyst for Hydrogen Generation from Hydrolysis of Sodium Borohydride. *Chem. Eng. J.* **2018**, 351, 48-55. DOI: 10.1016/j.cej.2018.06.082

[20] Kang, N.; Shen, R.; Li, B.; Fu, F.; Espuche, B.; Moya, S.; Salmon, L.; Pozzo, J.-L.; Astruc, D. Dramatic Acceleration by Visible Light and Mechanism of AuPd@ZIF-8-catalyzed Ammonia Borane Methanolysis for Efficient Hydrogen Production. *J. Mater. Chem. A* **2023**, 11, 5245-5256. DOI: 10.1039/D2TA08396E

[21] Feng, P. L.; Perry IV, J. J.; Nikodemski, S.; Jacobs, B. W.; Meek, S. T.; Allendorf, M. D. Assessing the Purity of Metal-Organic Frameworks Using Photoluminescence: MOF-5, ZnO Quantum Dots, and Framework Decomposition. *J. Am. Chem. Soc.* **2010**, 132, 15487-15489. DOI: 10.1021/ja1065625

[22] Liu, S.; Xiang, Z.; Hu, Z.; Zheng, X.; Cao, D. Zeolitic Imidazolate Framework-8 as a Luminescent Material for the Sensing of Ions and Small Molecules. *J. Mater. Chem.* **2011**, 21, 6649-6653. DOI: 10.1039/c1jm10166h

[23] Kumbhakar, P.; Singh, D.; Tiwary, C. S.; Mitra, A. K. Chemical Synthesis and Visible Photoluminescence Emission from Monodispersed ZnO Nanoparticles. *Chalcogenide Lett.* **2008**, 5 (12), 387-394.

[24] Parihar, V.; Raja, M.; Paulose, R. A Brief Review of Structural, Electrical and Electrochemical Properties of Zinc Oxide Nanoparticles. *Rev. Adv. Mater. Sci.* **2018**, 53, 119-130. DOI:10.1515/rams-2018-0009

[25] Biesinger M. C. Advanced Analysis of Copper X-ray Photoelectron Spectra. *Surf. Interface Anal.* **2017**, 49 (13), 1325-1334. DOI: 10.1002/sia.6239

[26] Yu, T.; Cai, Q.; Lian, G.; Bai, Y.; Zhang, X.; Zhang, X.; Liu L. Mechanisms Behind High CO₂/CH₄ Selectivity using ZIF-8 Metal Organic Frameworks with Encapsulated Ionic Liquids: A Computational Study. *Chem. Eng. J.* **2021**, 419, 129638. DOI: 10.1016/j.cej.2021.129638

[27] Moreno, I.; Dummer, N. F.; Edwards, J. K.; Alhumaimess, M.; Sankar, M.; Sanz, R.; Pizarro, P.; Serrano, D. P.; Hutchings, G. J. Selective Oxidation of Benzyl Alcohol Using In Situ Generated H₂O₂ over Hierarchical Au–Pd Titanium Silicalite Catalysts. *Catal. Sci. Technol.*, **2013**, 3, 2425-2434. DOI: 10.1039/C3CY00493G

[28] Hoover, J. M.; Ryland, B. L.; Stahl, S. S. Copper/TEMPO-Catalyzed Aerobic Alcohol Oxidation: Mechanistic Assessment of Different Catalyst Systems. *ACS Catal.* **2013**, 3 (11), 2599-2605. DOI: 10.1021/cs400689a

[29] van Beurden, K.; de Koning, S.; Molendijk D.; van Schijndel, J. The Knoevenagel Reaction: a Review of the Unfinished Treasure Map to Forming Carbon–Carbon Bonds. *Green Chem. Lett. Rev.* **2020**, 13 (4), 349-364. DOI: 10.1080/17518253.2020.1851398

[30] Sidhu, A.; Sharma, J. R.; Rai, M. Chemoselective Reaction of Malononitrile with Imine-Ones and Antifungal Potential of Products. *Indian J. Chem.* **2010**, 49, 247-250. DOI:10.1002/chin.201024075

[31] Maltsev, S. S., Mironov, M. A., Bakulev, V. A. Synthesis of Cyclopentene Derivatives by the Cyclooligomerization of Isocyanides with Substituted Benzyldenemalononitriles. *Mendeleev Commun.* **2006**, 16, 201-202. DOI: 10.1070/MC2006v016n04ABEH002354

[32] Amarante, S. F.; Freire, M. A.; Mendes, D. T. S. L.; Freitas, L. S.; Ramos, A. L. D. Evaluation of Basic Sites of ZIFs Metal Organic Frameworks in the Knoevenagel Condensation Reaction. *Appl. Catal. A: Gen.* **2017**, 548, 47-51. DOI: 10.1016/j.apcata.2017.08.006

[33] Shkoor, M.; Bayarl, R. DMAP-Catalyzed Reaction of Diethyl 1,3-Acetonedicarboxylate with 2-Hydroxybenzylideneindenediones: Facile Synthesis of Fluorenone-Fused Coumarins. *Synlett* **2021**, 32 (8), 795-799. DOI: 10.1055/a-1385-2345

[34] Mittelbach, M. An Improved and Facile Synthesis of 2-Amino-1,1,3-Tricyanopropene *Monatsh Chem.* **1985**, 116, 689-691. DOI: 10.1007/BF00798796

[35] Al-Mousawi, S. M.; Moustafa, M. S.; Hilmy Elnagdi, M. Green Synthetic Approaches: Solventless Synthesis of Polyfunctionally Substituted Aromatics as Potential Versatile Building Blocks in Organic Synthesis Utilizing Enaminones and Enaminonitriles as Precursors. *Green Chem. Lett. Rev.* **2011**, 4 (2), 185-193. DOI: 10.1080/17518253.2010.528049

[36] Hinde, C. S.; Webb, W. R.; Chew, B. K. J.; Tan, H. R.; Zhang, W.-H.; Hor, T. S. A.; Raja R. Utilisation of Gold Nanoparticles on Amine-Functionalised UiO-66 (NH₂-UiO-66)

Nanocrystals for Selective Tandem Catalytic Reactions. *Chem. Commun.*, **2016**, 52, 6557-6560.

DOI: 10.1039/C6CC02169G

Table of Content:

